Tréhu, A.M., Bohrmann, G., Torres, M.E., and Colwell, F.S. (Eds.)
Proceedings of the Ocean Drilling Program, Scientific Results Volume 204

11. Data Report: Grain-Size and Bulk and Clay Mineralogy of Sediments from the Summit and Flanks of Southern Hydrate Ridge, Sites 1244–1250, ODP Leg 204[1]

Eulàlia Gràcia,[2] Francisca Martínez-Ruiz,[3] Elena Piñero,[2]
Juan Cruz Larrasoaña,[4,5] Alexis Vizcaino,[2] and Gemma Ercilla[6]

ABSTRACT

We present grain size, granulometric statistical parameters, and calcium carbonate content of sediment samples from the summit and east and west flanks of southern Hydrate Ridge (Sites 1244–1250). These data are compared with magnetic susceptibility measurements from the same intervals. Bulk and clay mineralogy from Sites 1244 (east flank), 1247 (west flank), and 1250 (summit) are also presented. The integration of these data allows us to characterize the main sedimentary facies and composition of the Quaternary age sediments from southern Hydrate Ridge.

INTRODUCTION

Hydrate Ridge is a structural high located in the accretionary complex of the Cascadia subduction zone, offshore Oregon (USA) (Fig. F1A), where gas hydrates were recovered from the seafloor (e.g., Suess et al., 2001) and a ubiquitous bottom-simulating reflector (BSR) suggests widespread distribution of gas hydrates (Tréhu et al., 1999). During Ocean Drilling Program (ODP) Leg 204, nine sites were drilled on southern Hydrate Ridge (Tréhu, Bohrmann, Rack, Torres, et al., 2003; Tréhu et al., 2004b) (Fig. F1B). High-resolution three-dimensional mul-

F1. Hydrate Ridge and drill site locations, p. 11.

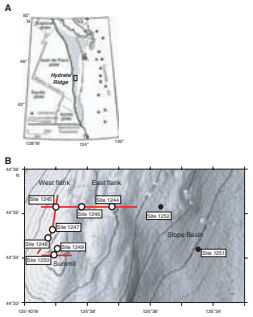

[1] Gràcia, E., Martínez-Ruiz, F., Piñero, E., Larrasoaña, J.C., Vizcaino, A., and Ercilla, G., 2006. Data report: Grain-size and bulk and clay mineralogy of sediments from the summit and flanks of southern Hydrate Ridge, Sites 1244–1250, ODP Leg 204. *In* Tréhu, A.M., Bohrmann, G., Torres, M.E., and Colwell, F.S. (Eds.), *Proc. ODP, Sci. Results,* 204, 1–19 [Online]. Available from World Wide Web: <http://www-odp.tamu.edu/publications/204_SR/VOLUME/CHAPTERS/110.PDF>. [Cited YYYY-MM-DD]
[2] Unitat de Tecnologia Marina, Centre Mediterrani d'Investigacions Marines i Ambientals (CSIC), 08003 Barcelona, Spain. Correspondence author: egracia@utm.csic.es
[3] Instituto Andaluz de Ciencias de la Tierra (CSIC)-Universidad de Granada, 18002 Granada, Spain.
[4] Laboratori de Paleomagnetisme, CSIC-Universitat de Barcelona, Institut de Ciències de la Terra "Jaume Almera," 08028 Barcelona, Spain.
[5] Departamento de Ciencias de la Tierra, Universidad de Zaragoza, 50009 Zaragoza, Spain.
[6] Institut de Ciències del Mar, Centre Mediterrani d'Investigacions Marines i Ambientals (CSIC), 08003 Barcelona, Spain.

Initial receipt: 28 January 2005
Acceptance: 11 August 2005
Web publication: 28 April 2006
Ms 204SR-110

tichannel seismic (MCS) reflection data from southern Hydrate Ridge (Tréhu et al., 2002) were available during Leg 204, illustrating the stratigraphic and structural complexity of the ridge as well as the relationship between subsurface reflectors and summit vents (Fig. F2).

The BSR, which is commonly interpreted to result from free gas underlying gas hydrate at the base of the gas hydrate stability zone, is observed in almost all seismic profiles. Other seismic reflectors with high amplitude, reflectivity, and good lateral continuation are referred to as Horizons A, B, B′, X, and Y (Tréhu, Bohrmann, Rack, Torres, et al., 2003) (Fig. F2). They were drilled and sampled during Leg 204 in order to investigate their nature and role in methane migration and gas hydrate formation. Horizon A corresponds to a 2- to 4-m-thick interval composed of multiple volcanic glass-bearing sediments and ash sequences (Shipboard Scientific Party, 2003a) and has been suggested as a conduit feeding gas from deep accretionary complex sediments to the surface vents and gas hydrate deposits (Torres et al., 2004; Tréhu et al., 2004a). Horizons B and B′ are pervasively faulted and located at the east flank of southern Hydrate Ridge (Fig. F2A). Horizon B is composed of multiple turbidites clustered into two 2-m-thick intervals. Horizon B′ is characterized by silt layers containing volcanic glass and ash (Shipboard Scientific Party, 2003a). Horizons X and Y do not seem to correlate with any apparent lithological change. Five lithostratigraphic units (Units I–V), ranging in age from early Pleistocene to Holocene (Tréhu, Bohrmann, Rack, Torres, et al., 2003), were defined on board and are also depicted on Figure F2.

Here we present results of grain size and carbonate content from seven Hydrate Ridge sites grouped into three environments: (1) summit, where active seafloor venting occurs (Sites 1249 and 1250); (2) east flank (Sites 1244 and 1246), characterized by the presence of Horizons B and B′; and (3) west flank (Sites 1245, 1247, and 1248), crossed by Horizons A and Y (Figs. F1, F2). Bulk and clay mineralogy were also obtained in these three environments at Sites 1244, 1247, and 1250. These new data allow us to define sediment texture and characterize the lithofacies and composition of southern Hydrate Ridge sediments in order to reconstruct sediment provenance and depositional environments. Furthermore, we will try to define a possible relationship between sedimentary texture and composition with the presence of gas hydrates. Analytical data presented here are depicted in Figures F3, F4, and F5 and compiled in Tables T1 and T2. Further data interpretation and discussions will be presented elsewhere (Piñero et al., 2004).

METHODS

Textural analysis and bulk and clay mineralogy were run with systematic sampling frequency of two samples per core except when crossing specific layers (e.g., Horizons A, B, and B′ and the BSR) defined on the three-dimensional MCS profiles (Tréhu et al., 2002; Tréhu, Bohrmann, Rack, Torres, et al., 2003). These intervals of interest were sampled at a rate of one sample per section. We collected samples (10-cm³ tubes) for sedimentology and geochemistry analyses and for rock magnetic measurements (7-cm³ cubes) (Gràcia et al., 2003; Larrasoaña et al., this volume) from the same stratigraphic intervals so that the data are directly comparable.

Grain-size analyses were performed using a settling tube for the coarse-grained (>50 µm) fraction (Gibbs, 1974) and SediGraph 5100 for

F2. Multichannel seismic profile line drawings, p. 12.

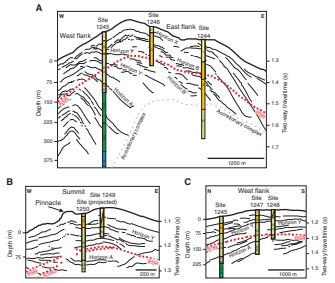

F3. Downhole variations, Holes 1249C and 1250C, p. 13.

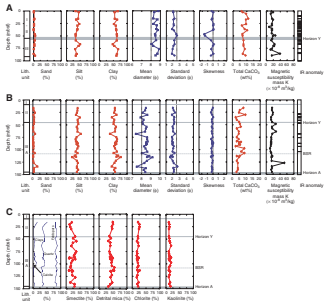

F4. Downhole variations, Holes 1244E and 1246B, p. 14.

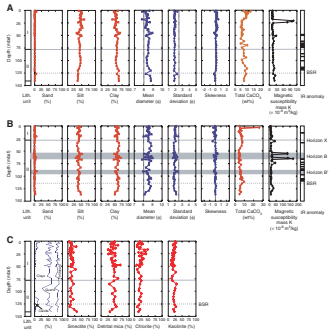

F5. Downhole variations, Holes 1245B, 1247B, and 1248C, p. 15.

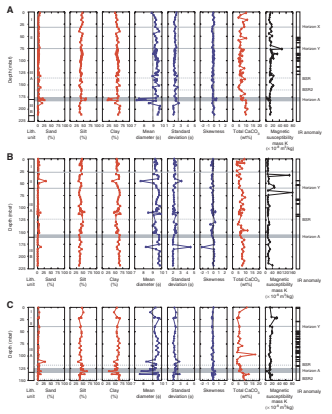

the silt and clay (<50 µm) fractions (Micromeritics, 1978). The division at 50 µm instead of 63 µm was established in order to have enough sediment samples for the settling tube, since a correct measurement requires a minimum 0.2 g of material. Although measured separately for each sample, sediment fractions were integrated in a single textural distribution using specific software. The SediGraph method determines the size distribution of particles as a function of the attenuation of an X-ray beam that crosses a transparent cell containing the samples in a dispersant suspension. The X-ray absorption is then converted into weight percentage of grain size on the basis of the sedimentation principle (Stoke's law of particles settling). This technique provides a rapid and accurate method (instrumental error = <1%) for grain-size analyses (e.g., Stein, 1985; Bianchi et al., 1999). We used the SediGraph because it is capable of sensing the total amount of material present and gives the whole size spectrum with satisfactory resolution >1 µm.

The grain-size distribution can provide information on particle size availability in the depositional system and on the type and competency of the processes operating in the system. Textural statistical parameters, such as mean size, standard deviation (sorting), kurtosis (peakness of the curve), and skewness (symmetry of the curve) are sensitive to environmental processes (e.g., Camerlenghi et al., 1995). Statistical parameters were calculated using the method of moments (McManus, 1988) on sample populations containing one-half ϕ-interval classes in all fractions. The Swan et al. (1979) sediment sorting classes were applied as follows: 0.5ϕ–0.8ϕ for well-sorted sediments, 0.8ϕ–1.4ϕ for moderately sorted sediments, 1.4ϕ–2ϕ for poorly sorted sediments, and 2ϕ–2.6ϕ for very poorly sorted sediments. Sand fraction and very coarse silt components (>50 µm) were identified using a binocular microscope, and relative abundances of components were estimated by counting a minimum of 300 grains per sample. We identified the following components: biogenic fraction (pelagic and benthic foraminifers, radiolarians, sponge spicules, etc.), light minerals (quartz, mica, and feldspar), heavy minerals, rock fragments, and diagenetic minerals (i.e., pyrite). Calcium carbonate content was determined using a Bernard calcimeter by the acid leaching method (Milliman, 1974).

Magnetic susceptibility was measured at the paleomagnetic laboratory of the Institute of Earth Sciences "Jaume Almera" (CSIC-UB) in Barcelona (Spain) (see **Larrasoaña et al.,** this volume). The low-field magnetic susceptibility was measured with a KLY-2 susceptibility bridge using a field of 0.1 mT at a frequency of 470 Hz and was normalized by the dry weight of the samples.

Bulk and clay mineral compositions were obtained by X-ray diffraction (XRD). For bulk mineralogy, the samples were air dried, ground in an agate mortar, and packed into Al sample holders for XRD analyses. For clay mineral analyses, the carbonate fraction was removed using acetic acid. Clays were deflocculated by successive washing with demineralized water after carbonate removal. The <2-µm fraction was separated by centrifuge at 900 rpm for 1.3 min, and the clay fraction was smeared onto glass slides. Separation of the clay fraction and preparation of the bulk samples for XRD analyses were performed following the international recommendations compiled by Kisch (1991).

X-ray diffractograms were obtained using a Philips PW 1710 diffractometer with CuK_α radiation and an automatic slit. Scans were run from 2° to 64°2θ for bulk sample diffractograms and untreated clay preparations and from 2° to 30°2θ for glycolated clay fraction samples. Diffractogram interpretations and semiquantitative analyses were performed

T1. Summary of grain-size results, p. 17.

T2. Summary of bulk and clay mineralogy, p. 18.

considering the integrated peak area using specific software (Xpowder, www.xpowder.com). The clay mineral proportion was estimated from the glycolated diffractogram. The 10-Å peak was used for illite, and the 7-Å peak was used for the total amount of chlorite and kaolinite, using the peak ratios at 3.54 Å and 3.58 Å, respectively, to differentiate these minerals. The 17-Å peak was used for smectites. The area between the illite peak at 10 Å and the smectite peak at 17 Å, which corresponds to the illite-smectite mixed layers, was not estimated because the peaks were usually masked by the smectite and illite peaks. The estimated semiquantitative analysis error for bulk mineralogy absolute values is 5%. In the case of clay mineralogy, the estimated semiquantitative analysis error ranges from 5% to 10%.

RESULTS

Summit of Southern Hydrate Ridge

Two sites were drilled at the summit of southern Hydrate Ridge. Site 1249 (778 m water depth), located on the summit, is characterized by massive gas hydrate deposits at the seafloor and methane venting into the water column (e.g., Suess et al., 2001). Site 1250 (792 m water depth) is located 100 m west of the summit and 100 m east of a highly reflective active carbonate chemoherm mound (Suess et al., 2001; Johnson et al., 2003) known as the Pinnacle (Figs. F1, F2B).

The uppermost 59.3 meters below seafloor (mbsf) of Hole 1249C and the uppermost 43.75 mbsf of Hole 1250C, corresponding to lithostratigraphic Units I and II (undifferentiated at Site 1249), are dominated by fine-grained silty clays to clays (mean size = 8.5ϕ) (Fig. F3). Relatively high values of calcium carbonate (11 wt% in Sample 204-1249C-4H-2, 6–8 cm [15.4 mbsf] and 9.5 wt% in Sample 204-1250C-4H-5, 50–52 cm [29.61 mbsf]) characterize these units and are probably associated with the presence of authigenic carbonates. Mousselike and soupy textures, related to gas hydrate dissociation, are abundant throughout Units I and II, especially at Site 1249, where the highest concentration of gas hydrates was encountered (Shipboard Scientific Party, 2003a). Large negative values of skewness were found in Samples 204-1249C-8H-2, 50–52 cm and 8H-4, 60–62 cm (46.51 and 49.55 mbsf, respectively), where as much as 2.24% of gravel sized sediments (iron sulfide nodules identified by scanning electron microscope) have been identified in a relatively fine grained matrix (>62% clay) (Fig. F3A).

Lithostratigraphic Unit III is characterized by the presence of gravity-driven deposits (i.e., turbidites and debris flows) interbedded with clays and silty clays (Fig. F3). A 13.5-m-thick clay clast dispersed in a muddy matrix debris flow disrupts toward the middle of this unit from 86.5 to 100 mbsf in Hole 1250C, with a texture of 1.09% sand, 37.68% silt, and 61.22% clay. The mean size of the matrix is 8.59ϕ (Sample 204-1250C-11H-5, 49–51 cm; 88.51 mbsf). Turbidite layers are mainly dominated by the silt fraction (mean size = 7.4ϕ), such as Sample 204-1250C-8H5, 50–52 cm (68.01 mbsf) with a grain-size distribution of 8% sand, 53.4% silt, and 38.6% clay. A turbidite base with 15.97% sand, 39.11% silt, and 44.92% clay (mean size = 7.48ϕ) was sampled at 204-1250C-17H-2, 50–52 cm (134 mbsf) (Fig. F3B). Turbidite samples are associated with moderate positive peaks (<28 × 10^{-8} m^3/kg) in the magnetic susceptibility record (Fig. F3A, F3B). The highest value of magnetic susceptibility in Hole 1249C (39 × 10^{-8} m^3/kg) corresponds to a hemipelagic sample

(204-1249C-13H-2, 50–52 cm; 86.01 mbsf) characterized by fine-grained texture (0.5% sand, 36.88% silt, and 62.6% clay) and collected from an interval containing abundant sulfide stains and gas-rich sediments (Fig. F3A). These data support the results presented by Larrasoaña et al. (this volume) on the relationship between rock magnetic properties of sulfides and presence of gas and hydrates. Similar data are obtained from Hole 1250C, where Sample 204-1250C-15H-5, 50–52 cm, located below the BSR (126.57 mbsf), shows the largest value in magnetic susceptibility (52×10^{-8} m^3/kg) with a silty clay texture (3.03% sand, 42.29% silt, and 54.67% clay) (Fig. F3B). No samples of Horizon A were available from Hole 1250C.

Bulk and clay mineral composition in Hole 1250C (Fig. F3C) revealed that the main mineral components at the summit of southern Hydrate Ridge are clays (30%–55%), quartz (25%–35%), and feldspars (15%–20%), with a minor amount of calcite (usually <5%) except for some carbonate-rich intervals at 16–20 mbsf corresponding to the uppermost sampled level and in the sediments above the BSR (~97 mbsf). The most abundant mineral observed in the clay association is detrital mica (35%–50%), whereas smectites, kaolinite, and chlorite are less abundant (Fig. F3C). Smectite content ranges from 10% to 30%, slightly lower in Unit II with respect to Unit III. The smectite content increases in Unit III close to Horizon A (140–145 mbsf) and corresponds with a decrease in detrital mica content.

East Flank of Southern Hydrate Ridge

Two sites were drilled at the east flank of southern Hydrate Ridge. Site 1244 (890 m water depth) is located ~3 km northeast of the summit, and Site 1246 (850 m water depth), near the crest, is located ~3 km north of the summit (Figs. F1, F2A). Only lithostratigraphic Units I and II were recovered from Hole 1244E, cored to 136 mbsf (Fig. F4), from where our samples were obtained.

Lithostratigraphic Unit I (0–77.6 mbsf in Hole 1244E and 0–21.7 mbsf in Hole 1246B) is dominated by dark greenish gray clay with occasional silty clay layers with a mean size of 8.45ϕ. The uppermost 20 mbsf of Unit I is characterized by a relatively high content of calcium carbonate showing peaks of 11 wt% in Hole 1244E at 2.57 mbsf (Sample 204-1244E-1H-2, 106–108 cm) and as much as 25 wt% in Hole 1246B at 3.51 mbsf (Sample 204-1246B-1H-3, 50–52 cm) (Fig. F4) that corresponds to near-surface authigenic carbonates. A large positive peak in magnetic susceptibility (up to 105×10^{-8} m^3/kg) is observed in Sample 204-1244E-4H-1, 50–52 cm (20.71 mbsf) and also in samples from Sections 204-1244E-4H-2 and 4H-3. High magnetic susceptibility values within this 3-m-thick interval do not seem to be associated with any evident textural change but are related to a compositional change (Fig. F4A). A fine-grained turbidite layer in Sample 204-1244E-7H-CC, 36–38 cm (50.83 mbsf) (0.54% sand, 49.61% silt, and 49.85% clay; mean size = 8.24ϕ) corresponds to a small positive peak of magnetic susceptibility (30×10^{-8} m^3/kg) (Fig. F4A).

Lithostratigraphic Unit II presents a grain-size distribution similar to Unit I except when crossing specific horizons. Hole 1246B Horizon B (from 54.1 to 65.22 mbsf) is characterized by the two largest peaks of the entire magnetic susceptibility data set (Fig. F4B). The younger peak, located at 55.6 mbsf, reaches values of 132×10^{-8} m^3/kg and corresponds to a clayey silt turbidite composed of 0.1% sand, 52% silt, and 47% clay with a mean size of 8ϕ (Sample 204-1246B-7H-3, 51–53 cm).

The older peak, located at 65.2 mbsf, has a higher magnetic susceptibility of 172 × 10^{-8} m^3/kg and corresponds to a silty clay interval composed of 0.47% sand, 42.21% silt, and 57.33% clay (Sample 204-1246B-8H-3, 51–53 cm) (Fig. F4B). This latter event is located just above an infrared thermal anomaly of –4°C (IR185) where gas hydrates were sampled (Shipboard Scientific Party, 2003a). Horizon B′, between 88 and 95 mbsf, is composed of two volcanic glass-bearing layers (Shipboard Scientific Party, 2003b). The upper layer (Sample 204-1246B-11H-1, 50–52 cm; 90.71 mbsf) is characterized by a textural distribution of 7.98% sand, 41.85% silt, and 50.17% clay with a mean size of 7.95ϕ and standard deviation of 2.4ϕ (Fig. F4B).

XRD data from Hole 1244E (Fig. F4C) show a mineral composition similar to the sediments recovered from the summit sites. The main mineral components are clays, quartz, feldspars, and calcite. The clay content ranges from 35% to 60%, quartz from 20% to 40%, and feldspars from 10% to 25%. Calcite content is below 5% through most of the sampled interval except for the samples located near the surface and above the BSR, where a significant increase likely related to fluid circulation and precipitation of authigenic carbonates is recognized. The clay mineral assemblage is also dominated by detrital mica (usually ranging from 30% to 60%), smectite (5%–30%), kaolinite (15%–30%), and chlorite (10%–30%) (Fig. F4C). Chlorite is relatively more abundant in Unit I than in Unit II, whereas kaolinite presents an opposite trend. Below the BSR and in the upper part of the site, a slight increase in smectite content corresponds to a decrease in the detrital mica values.

West Flank of Southern Hydrate Ridge

Three sites were drilled along the west flank of southern Hydrate Ridge following a north–south transect (Figs. F1, F2C). Site 1245 (870 m water depth) is located ~3 km northwest of the summit. Site 1247 (845 m water depth) is located ~800 m northwest of the summit. Site 1248 (830 m water depth) is located 300 m northwest of the summit (Fig. F1) in the middle of an area characterized by high backscatter and interpreted as related to the presence of authigenic carbonate resulting from fluid seafloor venting (Johnson et al., 2003) (Fig. F2C).

Lithostratigraphic Units I and II are undifferentiated at Site 1248 and are mainly composed of fine-grained silty clays (mean size = 8.28ϕ). Soupy and mousselike facies induced by gas hydrate dissociation are common above the BSR at Site 1248, located very close to the summit of Hydrate Ridge (Shipboard Scientific Party, 2003d) (Fig. F5C). At 33.39 mbsf, a large peak in the magnetic susceptibility record (>140 × 10^{-8} m^3/kg) corresponds to a 10-cm-long sulfide vein oblique to the stratification in a silty clay sediment composed of 2.38% sand, 36.93% silt, and 60.68% clay (Sample 204-1247B-5H-6, 128–130 cm) (Fig. F5B). Thin sand-silt turbidite layers are locally observed. One of these was sampled at 45.67 mbsf (Sample 204-1247B-7H-2, 61–63 cm) and contains 30.37% sand, 32.41% silt, and 37.22% clay with a mean size of 6.67ϕ. Seismic Horizon Y marks the boundary between Unit II and Subunit IIIA but does not seem to correspond to any major textural change, although a peak in the magnetic susceptibility data (47 × 10^{-8} m^3/kg) is measured for Sample 204-1245B-9H-1, 50–52 cm (76.5 mbsf) (Fig. F5A).

Near the top of Subunit IIIA at 69.02 mbsf, the largest peak in magnetic susceptibility (160 × 10^{-8} m^3/kg) is measured in a clay sample (1.44% sand, 34.73% silt, and 63.83% clay; mean size = 8.7ϕ) character-

ized by abundant sulfide stains (Sample 204-1247B-9H-5, 50–52 cm) (Fig. F5B). The highest value of calcium carbonate (16.7 wt%) is found at 96.67 mbsf in a clay-rich sample (Sample 204-1248C-11H-2, 50–52 cm; mean size = 8.61ϕ) (Fig. F5C). Turbidites are present as sandy silt layers with a textural distribution of 26.74% sand, 30% silt, and 43.26% clay with a mean size of 7.3ϕ and standard deviation of 2.7ϕ (e.g., Sample 204-1248C-12H-5, 50–52 cm; 112.12 mbsf) that correlate with a small peak in magnetic susceptibility (16.6×10^{-8} m^3/kg) (Fig. F5C). Only a few centimeters above this sample depth, a temperature anomaly of –4.7°C was recorded by the infrared camera (Anomaly IR162) (Shipboard Scientific Party, 2003d).

Seismic Horizon A was drilled at the three sites of the western flank of southern Hydrate Ridge. In Holes 1245B and 1248C, Horizon A corresponds to a series of volcanic glass-rich and ash sequences (Figs. F5A, F5C), whereas in Hole 1247B it corresponds to a clay clast-rich debris flow characterized by 0.76% sand, 33.35% silt, and 62.89% clay with a mean size of 8.7ϕ (Sample 204-1247B-21X-5, 50–52 cm; 160.41 mbsf), and is correlated with subdued reflectivity in the MCS data (Shipboard Scientific Party, 2003c). In Hole 1245B, Horizon A spans all of Core 204-1275B-21X with a textural distribution of 24.16% sand, 56.54% silt, and 19.3% clay with a mean size of 6.2ϕ and skewness of 0.5 (Sample 204-1245B-21X-4, 50–52 cm; 181 mbsf) (Fig. F5A). In Hole 1248C, Horizon A is characterized by a grain-size distribution of 11.35% sand, 63.67% silt, and 24.98% clay with a mean size of 6.75ϕ and skewness of 0.27 (Sample 204-1248C-14H-6, 47–49 cm; 130.72 mbsf) (Fig. F5C). Both coarse-grained ash-rich layers are correlated with exceptionally low values in the magnetic susceptibility record (3.72×10^{-8} and 1.8×10^{-8} m^3/kg for Sites 1245B and 1248C, respectively). From 5 to 20 m below Horizon A, a gravel-grained turbidite depicting a small peak in magnetic susceptibility is identified on the three west flank sites. This layer is characterized by 6.69% gravel, 4.69% sand, 34.75% silt, and 53.87% clay with a mean size of 7.24ϕ, standard deviation of 4.4ϕ, and skewness of –2.15 (Sample 204-1247B-23X-5, 102–104 cm; 180.13 mbsf) (Fig. F5B).

Regarding mineral composition, sediments from the west flank have similar components as those reported for Site 1244 on the east flank (Fig. F5D). Slight fluctuations are observed in bulk mineralogy with the exception of a very modest increase in calcite content with depth. The smectite content, ranging between 10% and 20% in Unit I, increases in Units II and III to 50%. Below the BSR, the smectite content increases downcore, reaching as much as 60% in the middle part of Subunit IIIB (Fig. F5D). Detrital mica content presents an opposite trend.

SUMMARY

Sediments from southern Hydrate Ridge show small fluctuation in grain-size distribution dominated by fine-grained (clay and silty clay) sequences locally interbedded with clayey silt to silty layers. Remarkable differences in sediment texture are only observed when specific intervals (Horizons A, B, and B′) are crossed. In general, sediments from southern Hydrate Ridge are fine grained characterized by an average mean size of 8.4ϕ. Statistical parameters indicate poorly sorted sediments with an average standard deviation of ~2ϕ and skewness of –0.08 corresponding to symmetrical curves. Calcium carbonate concentrations are generally low and range between 2.5 and 10 wt% (aver-

age = 6 wt%). High values as much as 25.9 wt% are associated with authigenic carbonates near the summit of southern Hydrate Ridge.

Bulk and clay mineral composition does not present significant changes between the summit and the flanks of the southern Hydrate Ridge sites. The bulk mineralogy is dominated by clays (30%–60%), quartz (25%–40%), feldspars (10%–25%), and minor amounts of calcite, which is usually below 5%. In the uppermost sampled sediments (2.5–16 mbsf) as well as above the BSR on the summit and east flank of southern Hydrate Ridge, the calcite content is as much as 20%. The clay mineral associations are dominated by detrital mica (average = 50%) and minor amounts of smectites, kaolinite, and chlorite ranging from 10% to 30%. Some noticeable trends are recognized in the smectite content, which usually increases downhole and below the BSR.

The main identified lithofacies comprise hemipelagic sediments, turbidites and ash layers, and debris flow deposits. The existence of coarser-grained horizons such as the ash-rich Horizon A may have played an important role in gas migration and gas hydrate formation (Tréhu et al., 2004a) as coarser-grained deposits are characterized by different packing structures and have a higher permeability that allow gas migration.

ACKNOWLEDGMENTS

We thank the captain, the crew, technicians, and fellow scientists aboard the *JOIDES Resolution* for their assistance during Leg 204. This research used samples and/or data provided by the Ocean Drilling Program (ODP). ODP is sponsored by the U.S. National Science Foundation (NSF) and participating countries under management of Joint Oceanographic Institutions (JOI), Inc. The Spanish Ministry of Science and Education (*Ministerio de Educación y Ciencia*) funded participation of E. Gràcia in ODP Leg 204 through grant REN2001-5262-E and analyses and sample processing through grant BTE2002-11698-E. E. Piñero benefits from *Ministerio de Educación y Ciencia* Ph.D. fellowship AP2003-2872, and J.C. Larrasoaña benefits from *Ministerio de Educación y Ciencia* "Ramon y Cajal" postdoctoral contract. We thank N. Maestro and B. Paracuellos (Institut de Ciències del Mar-Consejo Superior de Investigaciones Científicas), E. Abarca (Department of Mineralogy and Petrology-Universidad de Granada), and J. Montes (Instituto Andaluz de Ciencias de la Tierra-Consejo Superior de Investigaciones Científicas) for assistance with sedimentological and mineralogical analyses. We wish to thank reviewer Renata G. Lucchi and staff scientist Marta Torres whose constructive comments enabled us to improve our original manuscript.

REFERENCES

Bianchi, G.G., Hall, I.R., McCave, I.N., and Joseph, L., 1999. Measurement of the sortable silt current speed proxy using the Sedigraph 5100 and Coulter Multisizer IIe: precision and accuracy. *Sedimentology,* 46(6):1001–1014:10.1046/j.1365-3091.1999.00256.x

Camerlenghi, A., Lucchi, R.G., and Rothwell, R.G., 1995. Grain-size analysis and distribution in Cascadia margin sediments, northeastern Pacific. *In* Carson, B., Westbrook, G.K., Musgrave, R.J., and Suess, E. (Eds.), *Proc. ODP, Sci. Results,* 146 (Pt 1): College Station, TX (Ocean Drilling Program), 3–31.

Gibbs, R.J., 1974. A settling tube for sand-sized analysis. *J. Sediment. Petrol.,* 44:583–588.

Gràcia, E., Larrasoaña, J.C., Martínez-Ruiz, F., Ercilla, G., Vizcaino, A., and Garcia, M., 2003. Rock magnetic signature of gas hydrates in sediments from southern Hydrate Ridge (Cascadia Margin). *Eos, Trans. Am. Geophys. Union,* 84(46):F848. (Abstract)

Johnson, J.E., Goldfinger, C., and Suess, E., 2003. Geophysical constraints on the surface distribution of authigenic carbonates across the Hydrate Ridge region, Cascadia margin. *Mar. Geol.,* 202(1–2):79–120. doi:10.1016/S0025-3227(03)00268-8

Kisch, H.J., 1991. Illite crystallinity: recommendations on sample preparation, X-ray diffraction settings, and interlaboratory samples. *J. Metamorph. Geol.,* 9:665–670.

McManus, J., 1988. Grain size determination and interpretation. *In* Tucker, M. (Ed.), *Techniques in Sedimentology:* Oxford (Blackwell), 63–85.

Micromeritics, 1978. *Instruction Manual: Sedi Graph Particle Size Analyser,* Norcross, USA.

Milliman, J.D., 1974. *Marine Carbonates* (2nd ed.): Berlin (Springer-Verlag).

Piñero, E., Gràcia, E., Larrasoaña, J.C., Martínez-Ruiz, F., Ercilla, G., Vizcaino, A., Garcés, M., 2004. Sedimentología y magnetismo de sedimentos ricos en hidratos de gas de Hydrate Ridge (Margen de Oregón, ODP Leg 204): aplicación en estudios paleoclimáticos. *Geo-temas,* 6(5):149–152.

Shipboard Scientific Party, 2003a. Leg 204 summary. *In* Tréhu, A.M, Bohrmann, G., Rack, F.R., Torres, M.E., et al., *Proc. ODP, Init. Repts.,* 204: College Station TX (Ocean Drilling Program), 1–75. [**HTML**]

Shipboard Scientific Party, 2003b. Site 1246. *In* Tréhu, A.M, Bohrmann, G., Rack, F.R., Torres, M.E., et al., *Proc. ODP, Init. Repts.,* 204, 1–67 [CD-ROM]. Available from: Ocean Drilling Program, Texas A&M University, College Station TX 77845-9547, USA. [**HTML**]

Shipboard Scientific Party, 2003c. Site 1247. *In* Tréhu, A.M, Bohrmann, G., Rack, F.R., Torres, M.E., et al., *Proc. ODP, Init. Repts.,* 204, 1–84 [CD-ROM]. Available from: Ocean Drilling Program, Texas A&M University, College Station TX 77845-9547, USA. [**HTML**]

Shipboard Scientific Party, 2003d. Site 1248. *In* Tréhu, A.M, Bohrmann, G., Rack, F.R., Torres, M.E., et al., *Proc. ODP, Init. Repts.,* 204, 1–75 [CD-ROM]. Available from: Ocean Drilling Program, Texas A&M University, College Station TX 77845-9547, USA. [**HTML**]

Stein, R., 1985. Rapid grain-size analyses of clay and silt fraction by SediGraph 5000D: comparison with Coulter counter and Atterberg methods. *J. Sed. Petrol.,* 55(4):590–615.

Suess, E., Torres, M.E., Bohrmann, G., Collier, R.W., Rickert, D., Goldfinger, C., Linke, P., Heuser, A., Sahling, H., Heeschen, K., Jung, C., Nakamura, K., Greinert, J., Pfannkuche, O., Tréhu, A., Klinkhammer, G., Whiticar, M.J., Eisenhauer, A., Teichert, B., and Elvert, M., 2001. Sea floor methane hydrates at Hydrate Ridge, Cascadia margin. In Paull, C.K., and Dillon, W.P. (Eds.), *Natural Gas Hydrates: Occurrence, Distribution, and Detection.* Am. Geophysical Union, Geophys. Monogr. Ser., 124:87–98.

Swan, D., Clague, J.J., and Luternauer, J.L., 1979. Grain-size statistics II: evaluation of grouped moment measures. *J. Sediment. Petrol.,* 94:487–500.

Torres, M.E., Wallmann, K., Tréhu, A.M., Bohrmann, G., Borowski, W.S., and Tomaru, H., 2004. Gas hydrate growth, methane transport, and chloride enrichment at the southern summit of Hydrate Ridge, Cascadia margin off Oregon. *Earth Planet. Sci. Lett.,* 226:225–241.

Trehu, A.M., Bangs, N.L., Arsenault, M.A., Bohrmann, G., Goldfinger, C., Johnson, J.E., Nakamura, Y., and Torres, M.E., 2002. Complex subsurface plumbing beneath southern Hydrate Ridge, Oregon continental margin, from high-resolution 3-D seismic reflection and OBS data. *Fourth Int. Conf. Gas Hydrates*: Yokohama, Japan, 19023:90–96.

Tréhu, A.M., Bohrmann, G., Rack, F.R., Torres, M.E., et al., 2003. *Proc. ODP, Init. Repts.,* 204 [CD-ROM]. Available from: Ocean Drilling Program, Texas A&M University, College Station TX 77845-9547, USA. [**HTML**]

Tréhu, A.M., Flemings, P.B., Bangs, N.L., Chevallier, J., Gràcia, E., Johnson, J.E., Liu, C.S., Riedel, M., and Torres, M., 2004a. Feeding methane vents and gas hydrate deposits at south Hydrate Ridge. *Geophys. Res. Lett.,* 31:L23310.

Tréhu, A.M., Long, P.E., Torres, M.E., Bohrmann, G., Rack, F.R., Collett, T.S., Goldberg, D.S., Milkov, A.V., Riedel, M., Schultheiss, P., Bangs, N.L., Barr, S.R., Borowski, W.S., Claypool, G.E., Delwiche, M.E., Dickens, G.R., Gràcia, E., Guerin, G., Holland, M., Johnson, J.E., Lee, Y.-J., Liu, C.-S., Su, X., Teichert, B., Tomaru, H., Vanneste, M., Watanabe, M., and Weinberger, J.L., 2004b. Three-dimensional distribution of gas hydrate beneath southern Hydrate Ridge: constraints from ODP Leg 204. *Earth Planet. Sci. Lett.,* 222:845–862.

Tréhu, A.M., Torres, M.E., Moore, G.F., Suess, E., and Bohrmann, G., 1999. Temporal and spatial evolution of a gas-hydrate-bearing accretionary ridge on the Oregon continental margin. *Geology,* 27(10):939–942.

Figure F1. A. Plate tectonic setting of the Cascadia accretionary margin. Black outlined box shows location of Hydrate Ridge. **B.** Detailed bathymetric map (20-m contour) showing the location of Leg 204 drill sites on southern Hydrate Ridge. Open circles = sites presented in this data report, red lines = location of seismic profiles presented in Figure F2, p. 12 (Tréhu, Bohrmann, Rack, Torres, et al., 2003).

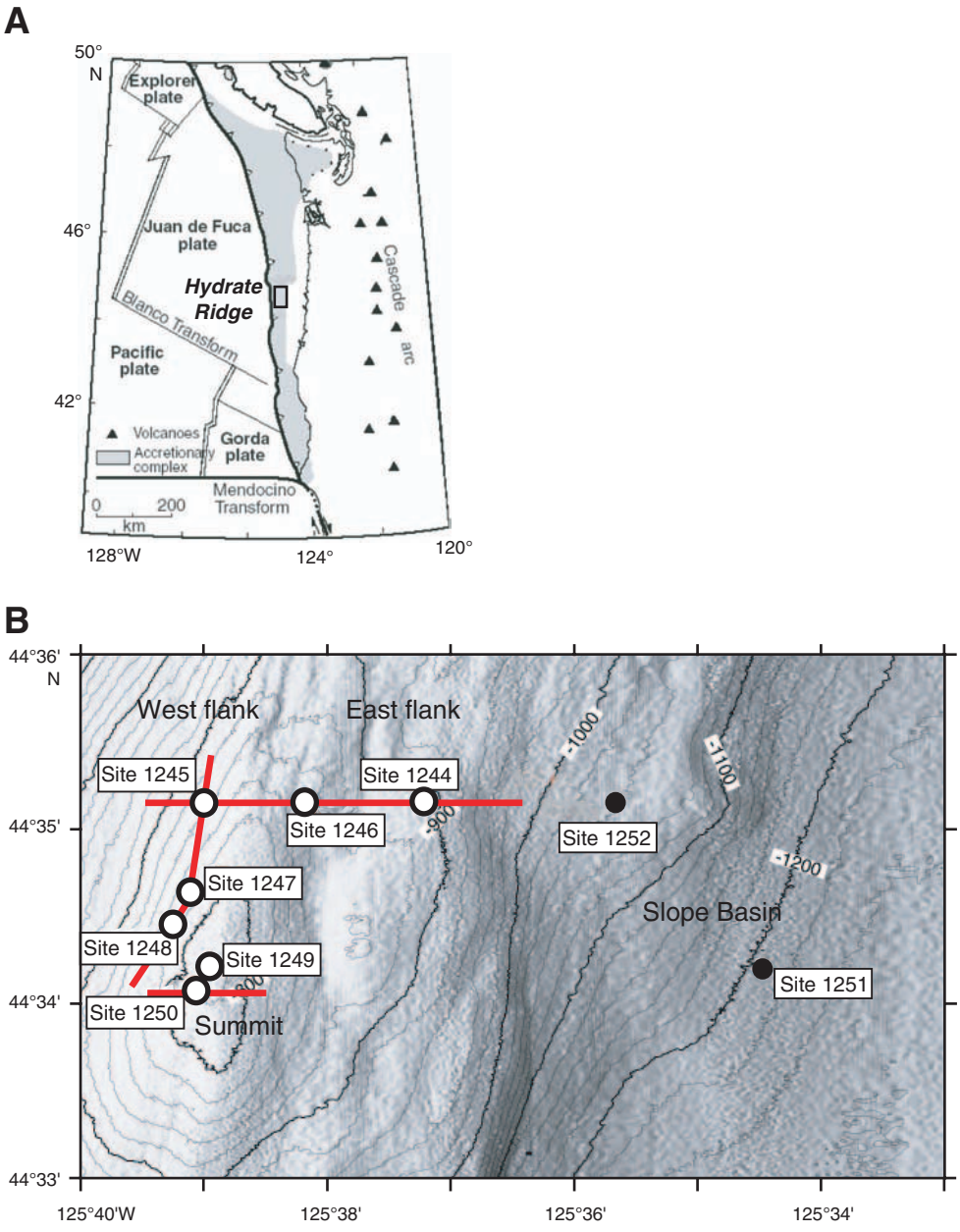

Figure F2. Line drawings from three-dimensional multichannel seismic profiles (Tréhu, Bohrmann, Rack, Torres, et al., 2003) corresponding to (**A**) west–east section across the northern part of southern Hydrate Ridge, (**B**) west–east section across the summit of southern Hydrate Ridge, and (**C**) north–south section along the west flank of southern Hydrate Ridge. The bottom simulating reflector (BSR) and main seismic horizons are indicated, as well as the Leg 204 borehole distribution in lithostratigraphic units of the drilled sites. Thick black rectangles = stratigraphic intervals studied in this data report.

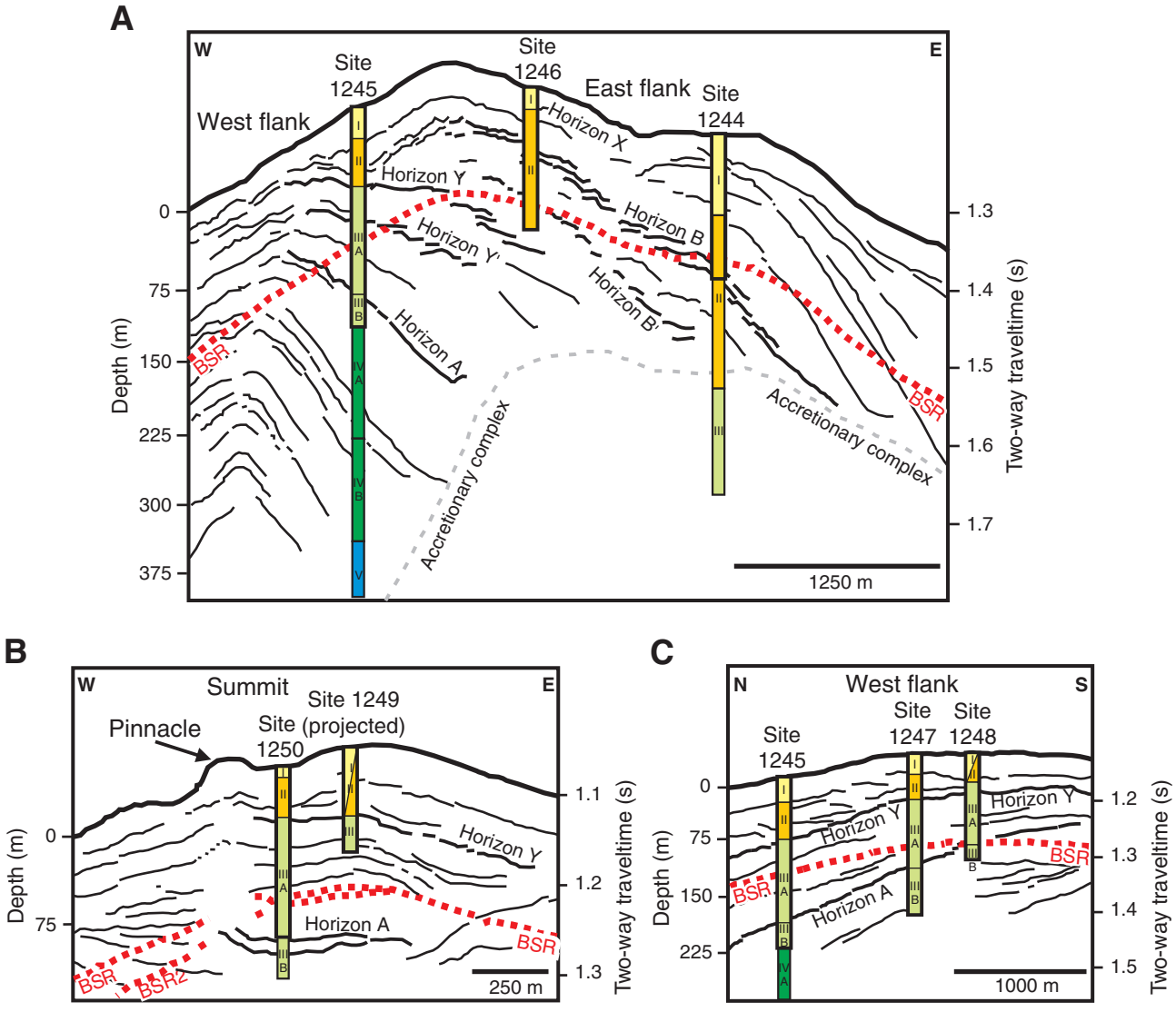

Figure F3. Downhole variations of grain size, textural statistical parameters, calcium carbonate, and magnetic susceptibility from (**A**) Hole 1249C and (**B**) Hole 1250C located at the summit of southern Hydrate Ridge. Lithostratigraphic units, main seismic horizons, and infrared (IR) thermal anomalies >1.7°C are also reported (after Shipboard Scientific Party, 2003a). (**C**) Downhole variations in bulk (calcite, clays, quartz, and feldspars) and clay (smectite, detrital mica, chlorite, and kaolinite) mineralogy from Hole 1250C. Semiquantitative analyses show changes or gradients in mineral abundances rather than absolute values. BSR = bottom simulating reflector.

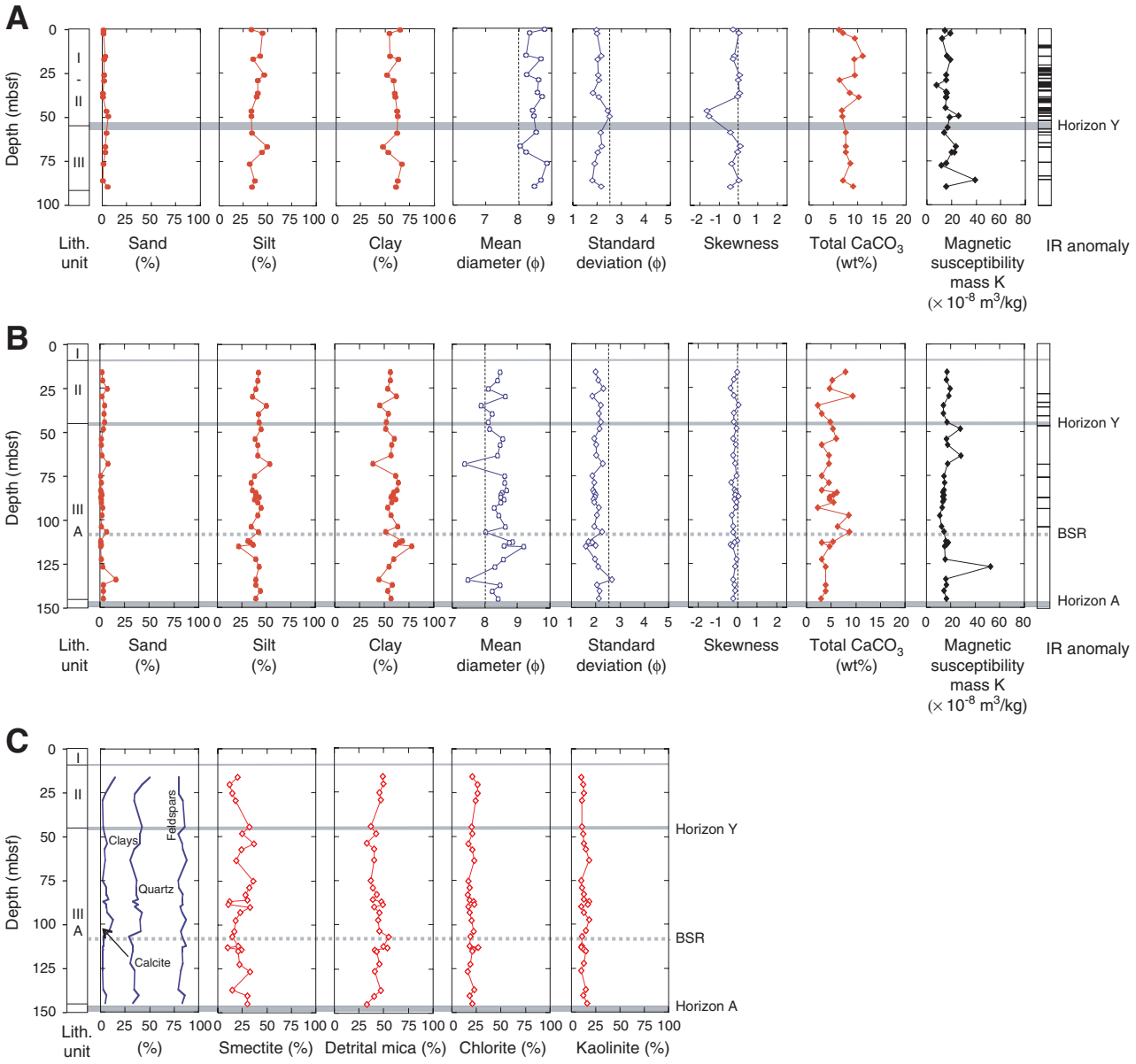

Figure F4. Downhole variations of grain size, textural statistical parameters, calcium carbonate, and magnetic susceptibility from (**A**) Hole 1244E and (**B**) Hole 1246B located on the east flank of southern Hydrate Ridge. (**C**) Downhole variations in bulk (calcite, clays, quartz, and feldspars) and clay (smectite, detrital mica, chlorite, and kaolinite) mineralogy in Hole 1244E. Semiquantitative analyses show changes or gradients in mineral abundances rather than absolute values. BSR = bottom-simulating reflector, IR = infrared.

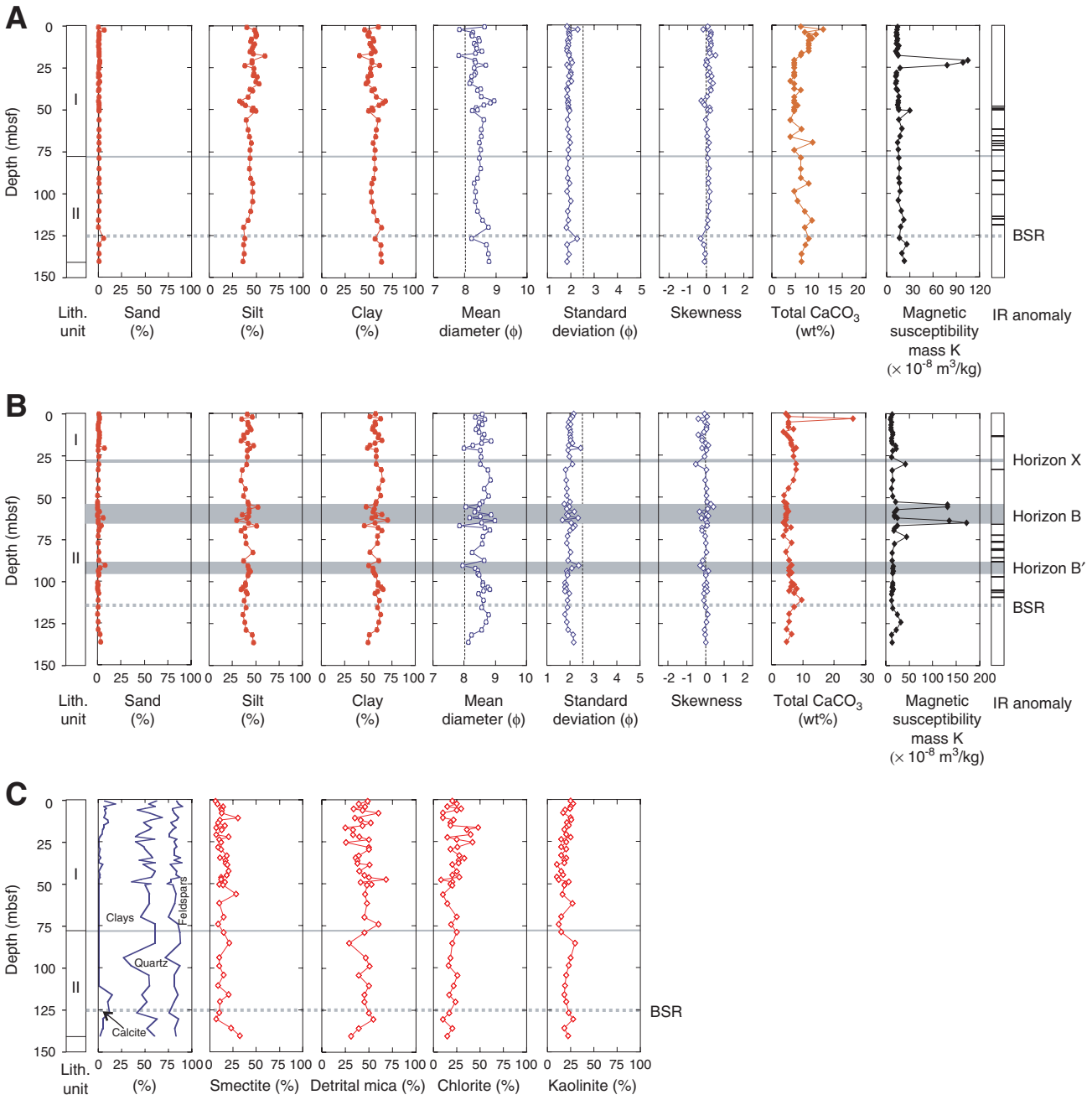

Figure F5. Downhole variations of grain size, textural statistical parameters, calcium carbonate, and magnetic susceptibility from (**A**) Hole 1245B, (**B**) Hole 1247B, and (**C**) Hole 1248C located on the east flank of southern Hydrate Ridge. BSR = bottom-simulating reflector, IR = infrared. (Continued on next page.)

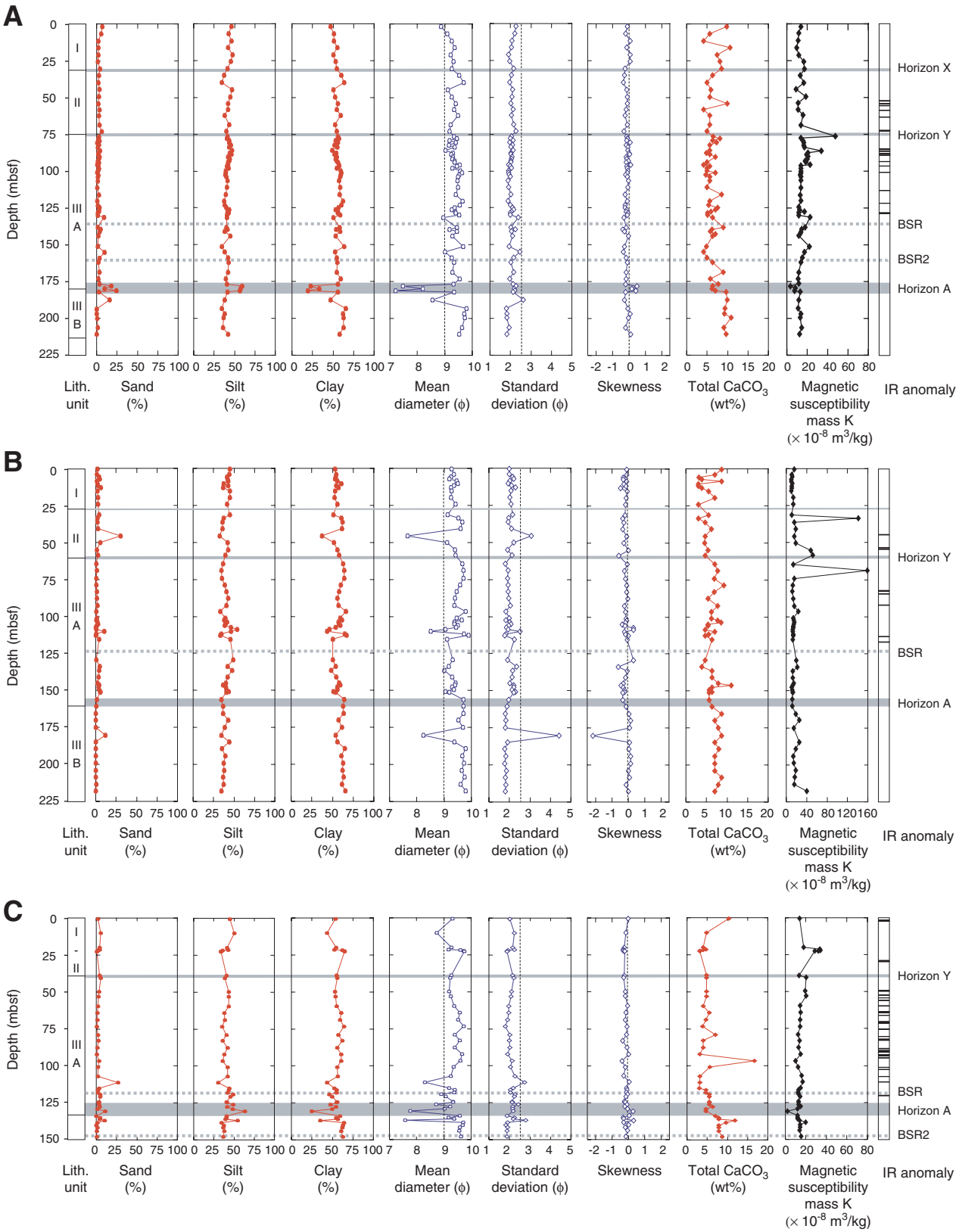

Figure F5 (continued.) (D) Downhole variations in bulk (calcite, clays, quartz, and feldspars) and clay (smectite, detrital mica, chlorite, and kaolinite) mineralogy in Hole 1247B. Semiquantitative analyses show changes or gradients in mineral abundances rather than absolute values.

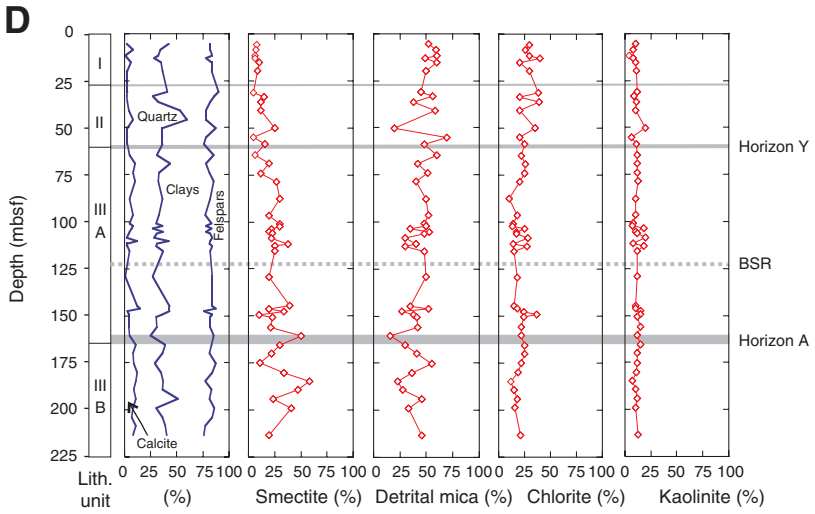

Table T1. Summary of grain-size results, statistical parameters, terrigenous and biogenic components of the sand fraction, and calcium carbonate in Holes 1244E, 1245B, 1246B, 1247B, 1248C, 1249C, and 1250C. (This table is available in an **oversized format.**)

Table T2. Summary of bulk mineralogy and clay mineral assemblages from Holes 1244E, 1247B, and 1250C. (Continued on next page.)

Core, section, interval (cm)	Depth (mbsf)	Bulk mineralogy (wt%)					Clay mineral assemblages (%)		
		Calcite	Clays	Quartz	Feldspars	Detrital mica	Smectites	Kaolinite	Chlorite
204-1244E-									
1H-1, 88–90	0.90	7	55	22	16	49	6	25	20
1H-2, 107–109	2.56	20	36	31	13	39	8	28	25
1H-3, 111–113	4.11	6	55	29	10	46	14	25	15
1H-4, 100–102	5.50	9	41	30	20	34	12	24	30
1H-5, 38–40	6.38	7	35	38	20	43	13	19	25
1H-6, 56–58	8.06	8	47	26	19	60	13	17	10
2H-2, 50–52	10.70	6	62	18	14	35	30	25	10
2H-3, 50–52	12.20	10	46	28	16	41	11	26	22
2H-4, 50–52	13.70	11	38	29	22	52	9	21	18
2H-5, 50–52	15.22	6	46	28	20	43	16	23	18
2H-6, 50–52	16.74	6	51	26	17	25	7	20	48
2H-7, 20–22	17.94	5	50	25	20	33	13	18	36
4H-1, 50–52	20.70	<5	40	32	24	33	7	20	40
4H-2, 50–52	22.20	2	38	36	24	40	20	25	15
4H-3, 50–52	23.70	<5	59	24	16	50	10	15	25
4H-4, 50–52	25.20	<5	39	41	19	26	12	20	42
4H-6, 50–52	28.20	<5	48	35	16	50	9	15	26
4H-7, 20–22	29.40	<5	48	31	19	50	12	20	18
5H-3, 50–52	33.15	<5	55	25	19	39	18	15	28
5H-4, 50–52	34.65	<5	55	30	12	36	11	20	33
5H-5, 50–52	36.15	<5	43	37	19	38	17	18	27
5H-6, 50–52	37.65	<5	60	28	11	38	17	18	27
5H-7, 20–22	38.52	5	43	29	23	51	19	10	20
7H-1, 132–134	42.52	<5	60	23	16	40	20	15	25
7H-3, 52–54	44.72	<5	57	24	16	45	18	17	20
7H-4, 42–44	46.12	<5	55	30	13	50	12	10	28
7H-5, 32–34	47.52	<5	45	32	22	68	12	12	8
7H-6, 23–25	48.93	<5	35	42	22	41	16	23	20
7H-7, 6–7	50.15	<5	55	18	26	53	10	19	18
7H-CC, 36–38	50.83	<5	49	30	20	48	14	18	20
9H-3, 63–65	56.23	<5	54	28	17	46	28	16	10
9H-7, 54–56	61.70	<5	54	27	18	48	10	27	15
10H-6, 22–24	69.82	<5	44	30	25	45	15	15	25
12H-1, 43–45	74.03	<5	60	24	15	60	9	12	19
12H-5, 23–25	78.93	<5	60	26	13	45	15	15	25
13H-2, 65–67	85.25	<5	60	27	12	29	21	30	20
14H-2, 48–50	94.10	<5	26	45	28	47	10	25	18
14H-5, 66–68	98.78	<5	34	52	13	51	10	23	16
16H-1, 42–44	104.52	<5	53	27	19	39	15	20	26
16H-5, 50–52	110.51	<5	54	26	19	50	9	19	22
17H-2, 89–91	115.99	15	32	38	15	45	20	18	17
17H-5, 52–54	120.12	10	42	29	19	45	11	20	24
18H-3, 57–59	126.67	12	29	35	24	50	10	23	17
18H-6, 54–56	130.39	5	58	23	14	55	7	28	10
19H-3, 87–89	136.07	5	47	30	18	39	23	18	20
19H-6, 83–85	140.53	<5	58	23	17	31	32	22	15
204-1247B-									
2H-2, 50–52	5.60	<5	40	40	18	52	8	10	30
2H-4, 50–52	8.60	8	48	26	18	59	7	8	26
2H-6, 50–52	11.60	<5	52	31	16	60	6	4	30
2H-7, 50–52	13.10	<5	50	25	22	49	6	8	40
3H-2, 50–52	15.10	6	48	29	17	60	10	10	20
3H-5, 50–52	19.60	<5	47	33	17	50	9	11	30
5H-5, 50–52	31.10	<5	49	38	10	45	5	12	38
5H-6, 128–130	33.37	<5	59	25	14	56	15	9	20
6H-2, 55–57	36.15	<5	50	29	18	38	12	11	39
6H-5, 50–52	40.60	<5	25	49	22	58	12	10	20
7H-5, 58–60	50.13	<5	51	33	13	20	25	20	35
8H-2, 47–49	55.07	<5	42	33	22	69	5	6	20
8H-4, 102–104	58.62	<5	40	33	24	48	16	11	25
9H-2, 50–52	64.51	5	54	26	15	60	6	12	22
9H-5, 50–52	69.01	10	34	34	22	42	20	12	26
10H-2, 50–52	74.10	8	48	25	19	51	12	12	25
10H-5, 50–52	78.60	10	53	22	15	40	27	13	20
11H-5, 47–49	87.68	5	46	31	18	50	30	10	10

Table T2 (continued).

Core, section, interval (cm)	Depth (mbsf)	Bulk mineralogy (wt%)					Clay mineral assemblages (%)		
		Calcite	Clays	Quartz	Feldspars	Detrital mica	Smectites	Kaolinite	Chlorite
12H-5, 50–52	96.61	8	44	25	23	52	20	10	18
13H-1, 50–52	101.10	5	53	25	17	48	30	8	14
13H-2, 62–64	102.35	8	42	28	22	50	30	7	13
13H-3, 50–52	103.73	7	56	20	17	35	22	18	25
13H-4, 47–49	105.20	5	41	32	22	53	20	10	17
13H-5, 45–47	106.18	<5	51	27	18	48	23	12	17
14H-2, 50–52	108.70	<5	56	26	16	30	22	20	28
14H-4, 50–52	111.70	<5	50	28	19	40	38	8	14
14H-5, 50–52	112.90	<5	54	27	16	30	25	18	27
15X-2, 50–52	115.60	5	45	32	18	48	25	12	15
18X-2, 50–52	129.30	<5	57	26	16	50	20	12	18
20X-1, 50–52	144.70	12	41	31	16	35	39	10	15
20X-2, 50–52	146.20	15	45	27	13	52	20	10	18
20X-3, 50–52	147.70	<5	33	40	24	27	34	15	24
20X-4, 50–52	149.20	<5	48	32	16	38	10	15	37
20X-5, 46–48	150.66	<5	52	26	18	41	23	12	24
21X-2, 50–52	155.90	<5	51	27	18	42	21	15	22
21X-5, 50–52	160.40	5	60	20	15	16	50	12	22
22X-2, 52–54	165.52	11	44	28	17	30	30	15	25
22X-5, 48–50	169.98	8	45	28	19	41	22	12	25
23X-2, 47–49	175.07	9	58	20	13	55	11	12	22
23X-5, 102–104	180.12	12	49	23	16	36	34	11	19
24X-2, 50–52	184.70	11	40	26	23	23	58	7	12
24X-5, 42–44	189.12	9	47	27	17	28	47	10	15
25X-2, 70–72	194.23	11	30	40	19	46	24	12	18
25X-6, 15–17	198.86	8	56	22	14	33	41	10	16
27X-2, 47–49	213.17	8	36	32	24	46	20	13	21
3H-2, 50–52	16.00	15	30	35	20	49	20	10	21
3H-5, 50–52	20.50	10	38	32	20	50	12	12	26
4H-2, 50–52	25.50	5	45	30	20	46	15	13	26
4H-5, 50–52	29.60	7	47	31	15	47	18	11	24
6H-2, 50–52	44.50	<5	44	39	14	37	32	11	20
6H-5, 54–56	48.31	<5	39	36	21	42	25	12	21
7H-2, 50–52	54.00	7	43	33	17	33	37	13	17
7H-5, 50–52	57.20	<5	50	30	16	40	24	15	21
8H-2, 50–52	63.50	5	58	25	12	40	19	18	23
10H-2, 65–67	75.15	<5	42	35	21	37	36	10	17
10H-5, 53–55	78.99	6	44	30	20	39	32	11	18
11H-1, 50–52	83.00	6	48	30	16	43	28	13	16
11H-3, 47–49	85.88	8	45	30	17	39	30	13	18
11H-4, 50–52	87.01	<5	50	30	17	48	12	18	22
11H-5, 49–51	88.50	6	46	32	16	49	11	17	23
11H-6, 50–52	89.96	6	46	29	19	40	33	10	17
12H-2, 48–50	93.13	7	41	35	17	46	23	13	18
12H-5, 50–52	97.53	13	47	27	13	44	18	18	20
13H-3, 42–44	103.81	9	41	32	18	46	17	15	22
13H-5, 60–62	106.99	<5	54	26	17	55	15	11	19
14H-1, 130–132	112.30	<5	54	30	13	50	21	11	18
14H-2, 50–52	113.00	<5	50	31	17	54	10	10	27
14H-3, 44–46	114.44	<5	50	30	17	41	24	13	22
14H-4, 33–35	115.26	<5	50	31	17	43	21	15	21
15H-2, 54–56	122.40	<5	54	28	16	46	22	13	19
15H-5, 50–52	126.56	<5	47	33	18	41	33	10	16
17H-4, 50–52	137.00	<5	45	31	21	47	15	15	23
19X-2, 50–52	140.50	6	47	33	14	40	30	12	18
19X-5, 50–52	144.95	5	50	28	17	33	30	16	21